Radiation Physics and Chemistry 176 (2020) 109077

Contents lists available at ScienceDirect

Radiation Physics and Chemistry

journal homepage: www.elsevier.com/locate/radphyschem

Effects of low-dose γ-irradiation on the structural, morphological, and optical properties of fluorine-doped tin oxide thin films

Bosco Oryema[a,b,*], Edward Jurua[a], Itani G. Madiba[c,d], Mlungisi Nkosi[c,d], Juliet Sackey[c,d], Malik Maaza[c,d]

[a] Department of Physics, Mbarara University of Science and Technology, P.O Box 1410, Mbarara, Uganda
[b] Department of Physics, Muni University, P.O Box 725, Arua, Uganda
[c] UNESCO-UNISA Africa Chair in Nanosciences and Nanotechnology, College of Graduate Studies, University of South Africa, P.O Box 392, Pretoria, South Africa
[d] NanoAfNet, Nanolaboratories, iThemba LABS-National Research Foundation of South Africa, P.O Box 722, Somerset West, Western Cape Province, South Africa

ARTICLE INFO

Keywords:
Fluorine-doped tin oxide thin films
Low-dose γ-irradiation
Structural property
Optical property
Surface morphology
Spacecraft thermal control coating

ABSTRACT

This paper presents the effects of low-dose γ-irradiation on the structural, morphological, and optical properties of Fluorine-doped tin oxide (FTO) thin films for application as a passive thermal control coating in future miniaturized lightweight spacecraft. Commercial-grade FTO films on glass substrate (Pilkington Ltd, UK) with a bulk density of 2.5 g/cm^3, sheet resistance of 12 Ω.sq^{-1}, coating thickness of 450 nm, optical band-gap of 3.80 eV, a carrier concentration of 1.50×10^{20} cm^{-3} and a mobility of 15 cm^2/Vs were irradiated at room temperature and atmospheric pressure using a ^{60}Co gamma source (with gamma energies of 1.17 MeV and 1.33 MeV) at iThemba Laboratory for Accelerator Based Sciences, Cape Town, South Africa. Each sample was exposed to γ-rays for a different span of time to achieve a series of different integrated absorbed doses of 20, 30, and 50 Gy, at a dose rate of 0.207 Gy/min. Evolution in structural properties of the films was characterized using a Bruker AXS D8 Advance XRD with Cu-Kα (λ = 1.54056 Å) scanned in the 2θ degree range of 20 – 80 degrees. Surface properties were analyzed using a VEECO Dimension 1100 AFM machine. Meanwhile, variations in optical transmittance of the films was investigated using a Cary 5000 UV-vis-NIR spectrophotometer of Varian, Inc. model internal DRA- 2500 in the wavelength range of 200 – 2500 nm. XRD results indicate an enhancement of crystallization after irradiation, slight peak shifts, and variations in crystallite sizes with increasing dose. Surface roughness decreased with increasing dose and the grain structures also seen to vary with dose. No significant variations in optical transmittance of the FTO films.

1. Introduction

Fluorine-doped tin oxide (FTO) is a transparent conducting oxide (TCO) with widespread applications that include touch panel contacts (Adjimi et al., 2018), gas sensors and electrodes in thin film solar cells (Lavanya et al., 2016), transparent light emitting diodes (Zeng et al., 2003), smart windows (Batzill and Diebold, 2005), thin film transistors and catalyst (Sharma et al., 2013), and flat panel displays and optoelectronic devices (Adjimi et al., 2018; Tuyen et al., 2019), among others. These applications are owed to FTO's desirable broad qualities such as high electrical conductivity combined with a high optical transparency in the visible spectrum range (Banyamin et al., 2014; Chowdhury et al., 2013; Zeng et al., 2003), high reflectivity in the infrared (IR) region despite being significantly transparent in the visible region (Banyamin et al., 2014; Chowdhury et al., 2013), high melting point, high mechanical strength and hardness, high electrochemical stability, good adherence to substrates, relatively a large bandgap (> 3 eV) (Sharma et al., 2013; Shi and Xu, 2017). Besides, FTO offers a relatively better economic favor as compared to indium-based tin-oxide (ITO) due to the relative abundancy and low cost of tin mineral (Chowdhury et al., 2013). All these qualities combined make FTO a potential candidate for heat management as a thermal control coating (TCC) on future long mission and cost effective miniaturized spacecraft such as the CubeSats.

A TCC is a passive thermal management system (PTMS) made of single- or multi-layer thin coating of select materials with high reflectivity in the IR region designed to protect internal equipment. This is achieved either by confining heat produced by the spacecraft electronic components within the spacecraft during extreme cold weather or reflecting heat fluxes from the Sun into space (Gilmore, 2002;

* Corresponding author. Department of Physics, Mbarara University of Science and Technology, P.O Box 1410, Mbarara, Uganda.
E-mail address: b.oryema@muni.ac.ug (B. Oryema).

https://doi.org/10.1016/j.radphyschem.2020.109077
Received 19 April 2020; Received in revised form 15 June 2020; Accepted 23 June 2020
Available online 01 July 2020
0969-806X/

Madiba et al., 2019). The TCCs enjoy the advantages of simplicity, low cost, energy saving, lightweight, and suitability for use in long-duration unmanned missions without servicing (Meseguer et al., 2012). However, mindfully the space environment is known to be one of the most extreme environments imaginable, where spacecraft are continuously bombarded by various species of ionizing radiations (protons, electrons, neutrons, γ-rays, and heavy charged particles) from galactic cosmic rays (GCRs) (Takahashi et al., 2018), trapped particles in the Van Allen belts (Pelton and Allahdadi, 2015), and the solar energetic particles (SEPs) (Chancellor et al., 2018, 2014; Jiggens et al., 2014). Gamma rays found in the space environment usually originate from the Sun, cosmic sources, and SEP and GCR interactions with neutral gas particles (Norberg, 2013; Pelton and Allahdadi, 2015).

It's well known that irradiating a metal oxide such as FTO with ionizing radiations lead to ionization damage and atomic displacement, leaving behind lattice defects in the form of vacancies (color centres or oxygen vacancies in oxides) (Abhirami et al., 2013; Tuğluoğlu, 2007), defect clusters, dislocations (Khamari et al., 2011; Lavanya et al., 2016; Sen et al., 2019b), grain growth, fragmentation, and swelling (Madiba et al., 2017). Additional defects such as phase transformations, amorphization and chemical effects (cation reduction, anion loss) can also occur in materials that are highly susceptibility to damage accumulation (Lavanya et al., 2016; Madiba et al., 2017). The type and degree of defects that a material undergoes strongly depend on the type, dose and energy of the radiation, and on several parameters of the material involved like atomic mass, thickness, density of the host atoms and temperature of the material during irradiation (Khamari et al., 2011; Kumari et al., 2014; Sen et al., 2019b; Tuğluoğlu, 2007). Gamma-rays cause defects as it interacts with matter through three distinct processes, namely Compton scattering, the photoelectric effect and pair production (Lavanya et al., 2016; Souli et al., 2019). Ionization damage occurs when a γ-ray photon traversing a material interacts with and knocks-out an electron(s) from its shell, creating electron-hole pairs. The primary knock-out electrons gain sufficient amount of energy to subsequently displace other target atoms through secondary and higher-order collision processes. This can cause a sequence of energy sharing collisions and displacement cascades, which could lead to a large variety of structural modifications (Arshak and Korostynska, 2006). These defects can degrade the structural, physical, chemical, optical, and electrical properties of the irradiated material, which may in turn strongly affect its performance (Arshak et al., 2004; El-Nahass et al., 2018; Lavanya et al., 2016; Maity and Sharma, 2011; Sen et al., 2019b). However, positive effects such as improvement in electrical conductivity, crystallinity and increase in electron density have also been reported (Kumari et al., 2014).

Thus, proper understanding of evolutions in structural, morphological, and optical properties of FTO is vital for qualifying it for passive thermal control coating in future spacecraft. Currently, only a few studies have reported modifications in the properties of tin oxide-based thin films under irradiation. Kaya et al., studied γ-irradiation induced modifications on the structural, morphological, electrical, and electrochemical properties of n-SnO_2/p-Si heterojunction diodes. Their study revealed improved crystallographic structure, smoother surface roughness, reduced capacitance, and reduced interface state density of SnO_2 following γ-irradiation exposure (Kaya et al., 2019). Kondkar and Rukade investigated phase transitions and morphological modifications in SnO_2 thin films irradiated with 75 MeV Au^{7+} ions. Their study also showed enhanced crystallinity of the films, increased grain size, and nanocluster formation with increase in the ion fluence **(**Kondkar and Rukade, 2017**)**. Singh et al., investigated the effects of swift heavy ion (Ag^{+9}) irradiation on the structural, morphological, optical and electrical properties of FTO. They observed decreased crystalline sizes, increased sheet resistivity, and reduced optical transmittance of the films with increasing ion fluences (Singh et al., 2015). Rani et al., investigated the effects of swift heavy ion (Ni^{+}) irradiation on the structural, optical, and gas sensing properties of un-doped SnO_2 thin films. Their study showed an enhancement of crystallinity and systematic change of stress in the SnO_2 lattice at low fluence, but decrease in crystallinity at high fluence (Rani et al., 2008). Sharma et al., studied structural and surface microstructure evolutions in SnO thin films under 150 MeV Au beam irradiation (Sharma et al., 2013). Lavanya et al., reported notable modifications of the properties of SnO_2 nanoparticles following exposure to γ-radiation at different doses. They also observed decreased crystallinity of the samples irradiated with 50 kGy and 100 kGy, and increased crystallinity in sample irradiation with 150 kGy of γ-rays (Lavanya et al., 2016). Abhirami et al., reported pronounced variations in crystallinity, reductions in optical transmittance and electrical resistance of SnO thin films under various doses of γ-irradiation (Abhirami et al., 2013). To the best of our knowledge, no study has reported the effects of γ-irradiation on the properties of FTO. Hence, the present study investigates the evolutions in structural, morphological and optical properties of FTO thin films irradiated at room temperature and atmospheric pressure using γ-rays from a ^{60}Co source.

2. Materials and methods

2.1. Sample irradiation

The material experimentally investigated in this study was commercial-grade FTO thin film on glass substrate (Pilkington Ltd, UK) with a bulk density of 2.5 g/cm^3, sheet resistance of 12 Ω.sq^{-1}, coating thickness of 450 nm, optical band-gap of 3.80 eV, a carrier concentration of 1.50 × 10^{20} cm^{-3} and a mobility of 15 cm^2/Vs. Four samples of uniform sizes (1 cm × 1 cm) were cut from the main sample and cleaned in a sonicator for 30 min using acetone and distilled water. One set was used as a control sample or as-deposited sample and the other three were irradiated at room temperature and atmospheric pressure using a ^{60}Co gamma source (with gamma energies of 1.17 MeV and 1.33 MeV). The irradiation experiment was conducted at iThemba Laboratory for Accelerator Based Sciences, Cape Town, South Africa. Each sample was exposed to γ-rays for a different span of time to achieve a series of different integrated absorbed doses of 20, 30, and 50 Gy, at a dose rate of 0.207 Gy/min.

2.2. Characterization techniques

Structural analysis of both the irradiated and un-irradiated films was performed at room temperature using a Bruker AXS D8 Advance X-ray diffractometer (XRD) with Cu-Kα (λ = 1.54056 Å) radiation in the 2θ degree range of 20–80°. A VEECO Dimension 1100 Atomic Force Microscopy (AFM) operated in tapping mode was used to provide information about the surface properties of the samples. Evolution in optical property of the samples was investigated by measuring optical transmittance of the irradiated and un-irradiated films using a Cary 5000 ultraviolet–visible–near infrared (UV–vis–NIR) spectrophotometer of Varian, Inc. model internal DRA- 2500 operated in the wavelength range of 200–2500 nm.

3. Results and discussion

3.1. Structural evolution of FTO under γ-ray exposure

3.1.1. General diffraction peak observations

The XRD patterns for both the irradiated and original un-irradiated samples are shown in Fig. 1. It can be observed from Fig. 1 that both samples exhibited similar XRD spectral patterns with diffraction peaks corresponding to the (110), (101), (200), (211), (220), (310), (301), and (321) planes at 2θ diffraction angles of 26.5°, 33.7°, 37.7°, 51.5°, 54.5°, 61.5°, 65.5°, and 78.3° respectively. When compared with patterns from the standard powder diffraction card JCP2 No. 41–1445, these diffraction patterns are found to be polycrystalline tetragonal

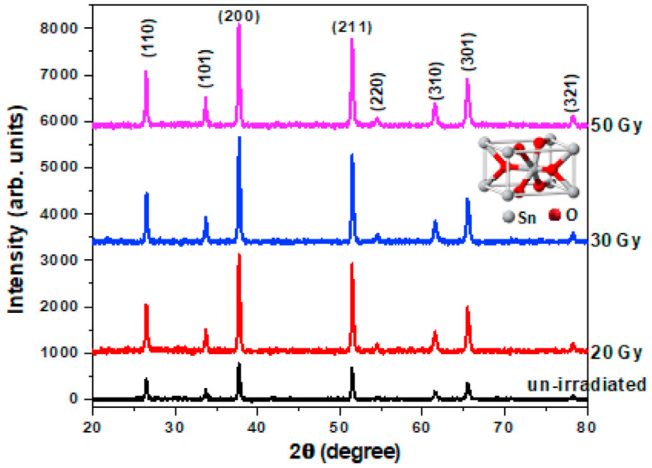

Fig. 1. XRD patterns of un-irradiated and of the γ-irradiated FTO samples at different doses.

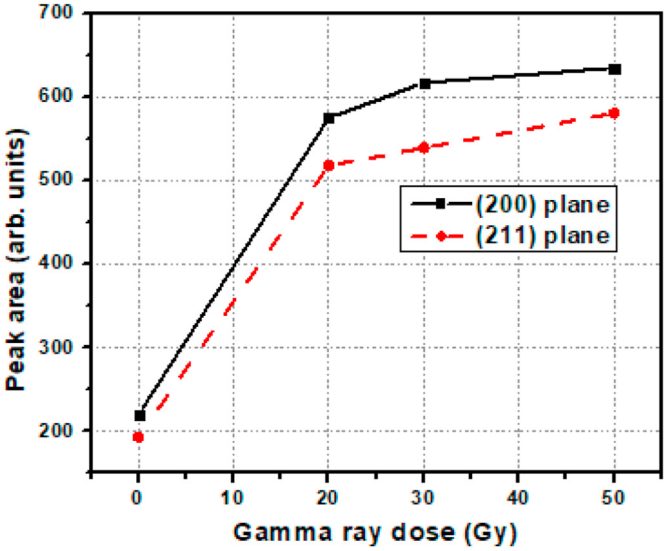

Fig. 2. Variations in peak area of the film before irradiation (0 Gy) and after irradiation with 20, 30, & 50 Gy of γ-rays.

rutile phase of the cassiterite SnO_2 (Adjimi et al., 2018). Fig. 1 also shows that the most preferred diffraction spectra of both the irradiated and un-irradiated films are the (200) and (211) planes. This indicates that a large proportion of crystals in the samples are textured within the (200) and (211) crystallographic orientations.

Comparing XRD measurements of the original un-irradiated sample with those of irradiated samples depicts no evident complex crystallographic changes such as amorphous phase transformations in the irradiated samples. Furthermore, there were no observed new peaks of SnO_2, and no diffraction patterns corresponding to fluoride phases such as SnF_2 despite the presence of fluorine dopant in the films. The absence of any unwanted peaks confirms the high purity of the product as well as no interfacial diffusion of fluorine from the FTO towards the substrate. The nonexistence of fluoride phases could have been either because they were overlapped with SnO_2 peaks, or the γ-ray doses used were not adequately high to generate or enhance crystallinity of fluorine phases to visible levels (Samad et al., 2011). It can also be speculated that during the FTO film preparation and doping processes, the fluorine dopant atoms could have replaced oxygen atoms in the SnO_2 films without necessarily forming secondary crystalline fluoride phases (Banyamin et al., 2014; Deyu et al., 2019; Samad et al., 2011).

It's also observed from Fig. 1 that increasing the γ-ray dose caused significant structural modifications of the FTO films, manifested as enhancement in spectral line intensities of the films with increasing dose. This is confirmed further by comparing variations in peak areas for the two most preferred planes of the irradiated and un-irradiated samples as shown in Fig. 2. As observed from Fig. 2, peak area increased with increasing γ-ray dose, and since peak area is synonymous with peak intensity (Baccini, 2019), the observed increase in peak area implies enhancement in crystallinity of the films. Enhancement in crystallinity of tin oxide films following γ-irradiation have been reported in previous studies such as (Abhirami et al., 2013; Kaya et al., 2019; Lavanya et al., 2016). Also, previous studies (Kondkar and Rukade, 2017; Rani et al., 2008) reported improvement in spectral line intensities of tin oxide films irradiated with swift heavy ions.

The observed enhancement in spectral line intensity is attributed to the energy transferred to SnO_2 lattice by γ-ray photons (Rani et al., 2008). Depending on its energy, a γ-ray photon interacts with matter and transfers part or whole of its kinetic energy to the target atoms causing trails of ionizations along its paths (Adrovic, 2012). The resultant primary and secondary electrons transfer their energies to atomic lattices through the electron–phonon coupling, triggering lattice vibrations and thus local temperature rise within the samples (Mirzayev et al., 2018; Sen et al., 2019b). This local rise in temperature releases local stress/strain between the grains and cause atom rearrangements, grain aggregation, and increased crystal densification (Duinong et al., 2019; Kaya and Yilmaz, 2018; Narula and Chauhan, 2018). The end result is increased number of diffracting particles and thus, enhanced probability of the film crystals to interact with the XRD beams (El-Nahass et al., 2018; Kadziołka-Gaweł et al., 2018; Kaya and Yilmaz, 2018; Lavanya et al., 2016). This could have contributed to the enhancement in crystallinity observed in this study. Since the total amount of energy deposited in the lattice increases with dose, the XRD peak intensities of the FTO films also increased with increasing γ-ray dose as observed in Fig. 2.

3.1.2. XRD peak shifts

In order to investigate possible shifts in diffraction peak positons of FTO film following γ-irradiation, magnified XRD pattern of the most preferred planes (200) and (211) were used as representatives. Fig. 3 shows the variations in diffraction peak intensity of FTO film with γ-ray dose. For the (200) plane, slight peak shift towards higher 2θ angles was observed for the 20 Gy and 30 Gy irradiated samples. However, at 50 Gy, the peak is seen to shift towards lower 2θ angles. The same observations apply to the (211) plane, except that no peak shift was observed for the 20 Gy irradiated sample. These shifts in peak positions

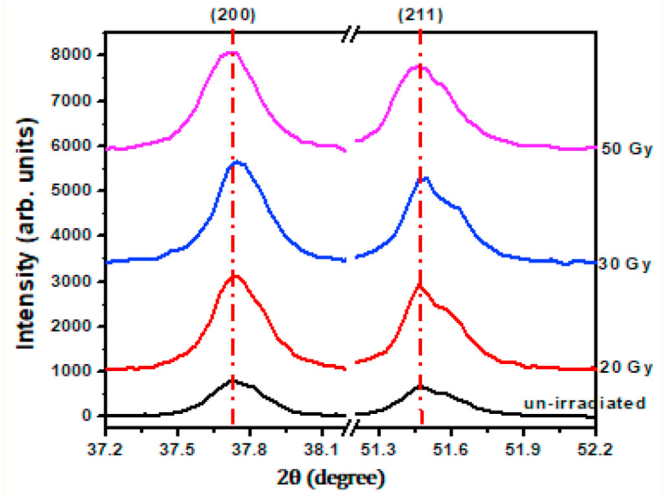

Fig. 3. Shifts in diffraction peak positions of the preferred lattice planes (200) and (211).

Table 1
Structural parameters of preferred FTO peaks with different absorbed γ-ray doses.

Absorbed dose (Gy)	2θ (°)	(*hkl*)	*d*-spacing (nm)	β (x10^{-3}) in rad	*D* (nm)	δ (x10^{-4} lines/nm^{-2})	ε (x10^{-3})	Lattice constants (Å)	
								a	***c***
un-irradiated	37.746	200	0.23814	4.765	32.13	9.6946	3.485	4.7567	3.2075
	51.509	211	0.17728	5.158	31.19	10.291	2.673		
20	37.750	200	0.23811	4.741	32.29	9.5974	3.467	4.7544	3.2108
	51.509	211	0.17728	5.125	31.38	10.161	2.656		
30	37.759	200	0.23805	4.706	32.54	9.4539	3.440	4.7526	3.2125
	51.518	211	0.17725	5.147	31.25	10.246	2.667		
50	37.717	200	0.23831	4.905	31.21	10.273	3.590	4.7602	3.2075
	51.483	211	0.17736	5.300	30.34	10.869	2.748		

are attributed to atomic displacement and to the presence of strain in the lattice structure of FTO under irradiation exposure (Kaya et al., 2019; Sen et al., 2019a, 2019b). Atomic displacement is the rearrangement in lattice structure attributed to temperature rise within a material. It causes lattice imperfections and distortions such as dislocations, vacancies, self-interstitial atoms, and point defect migration within the material (Alekperov et al., 2019; Madiba et al., 2017; Narula and Chauhan, 2018). The presence of these defects could have led to variations of peak positions observed in Fig. 3. Much as the γ-ray energy used in this study was able to slightly dislocate or shift the FTO atoms from their original positions, it is not sufficient to cause phase transformation in the film.

3.1.3. Lattice spacing

The current study also investigated the effects of γ-irradiation on structural parameters such as lattice spacing, grain size, lattice strain, dislocation density, and lattice constants. The calculated values of these structural parameters are listed in Table 1. The lattice spacing (*d*) of the (200) and (211) planes before and after irradiation were calculated using the Bragg's formula, $n\lambda = 2d\sin\theta$ and presented against γ-ray dose as shown in Fig. 4. It's clearly seen from Fig. 4 that lattice spacing for both the (200) and (211) planes decreased with increasing γ-ray dose up to 30 Gy, and then sharply rose when the dose was increased to 50 Gy. The observed decrease in *d* is indicative of the existence of irradiation induced compressive stress defects which icepacks the crystals and shrinkages the spacing between lattice points (Banyamin et al., 2014; Madiba et al., 2019). The presence of compressive stress and reduction in lattice spacing account for the observed shift in diffraction peak positions of the 20 Gy and 30 Gy irradiated films towards higher 2θ values (Wang et al., 2019) as shown in Fig. 3. Conversely, increase in lattice spacing indicates expansion (tensile stress) rather than compressive stress (Madiba et al., 2019; Wang et al., 2019).

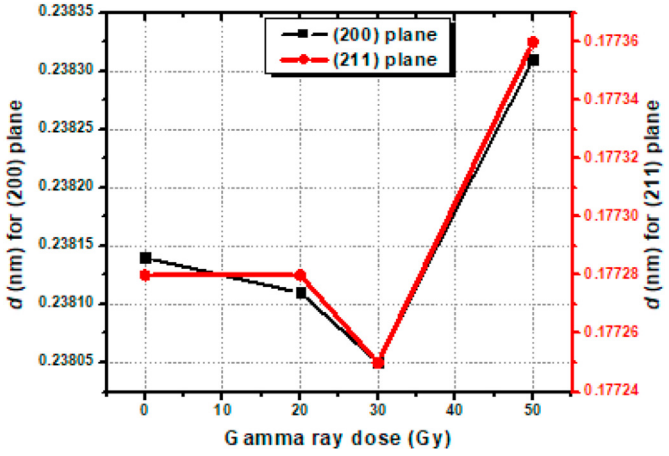

Fig. 4. Variations in lattice spacing of FTO films with γ-ray doses.

3.1.4. Grain size

Grain size or crystallite size is the measure of the size of a coherently diffracting domain in the sample (Bindu and Thomas, 2014). The average grain size (*D*) for the preferred diffraction planes (200) and (211) were calculated using Scherrer equation (Bindu and Thomas, 2014);

$$D = \frac{k\lambda}{\beta\cos\theta},$$

where, λ is the wavelength of the diffracted X-ray (λ = 1.5406 Å), θ is the Bragg angle, β is the full width at half maximum (FWHM) of the diffraction peaks in radians, and *k* is the constant of proportionality (also known as the Scherrer constant). The value of *k* varies from 0.62 to 2.08 depending on the shape and size distribution of the crystallites. The most commonly used value of *k* is 0.94 (Langford and Wilson, 1978). Thus, in this study, 0.94 was used as the Scherrer constant to determine the crystallite sizes of both un-irradiated and γ-irradiated FTO films. The calculated *D* values are shown in column 6 of Table 1. Variations in grain size and FWHM with γ-ray dose are shown in Fig. 5. Generally it's observed that for the (200) peak, grain size increased for samples exposed to 20 Gy and 30 Gy, and later swiftly dropped when γ-ray dose was increased to 50 Gy. On the other hand, for the (211) plane, the grain size increased for samples exposed to 20 Gy and gradually reduced when the doses were increased to 30 Gy and 50 Gy. FWHM exhibited inverse proportionality to grain sizes. The observed increase in grain size is associated with alterations in the lattice volume and lattice parameters due to the γ-irradiation induced local heating of the FTO nanoscale particles through lattice-phonon scattering (Sen et al., 2019a). The local heating crumbles the grain boundaries and releases pre-existing strain between grains and leads to migration of defects and atoms and thus consequently, formation of larger grain clusters due to coalition or agglomeration of smaller grains (Kaya et al., 2019; Kumar et al., 2016). On the other hand, the reduction in grain size can be attributed to irradiation induced voids due to fragmentation or splitting of large size grains (Alyamani and Mustapha, 2016). Grain fragmentation occurs as a result of vast temperature increase as well as rapid buildup of pressure waves and thermal spikes above the melting point of the host material (Kumar et al., 2016). Generally, the results suggest that at lower doses, γ-irradiation does constrictive work towards crystallization and then destructive work (fragmentation or creation of defects) at higher doses.

3.1.5. Lattice strain and dislocation density

Lattice strain is responsible for XRD line broadening which are caused by formation of crystal defects such as imperfections and distortions. Its presence in a sample strongly affects the sample's Bragg peak distribution, intensity, and position (Baccini, 2019). The average lattice strain (ϵ) can be calculated using the Stokes–Wilson equation (Sen et al., 2019b) as;

$$\varepsilon = \frac{\beta}{4\tan\theta},$$

On the other hand, dislocation density provides information about

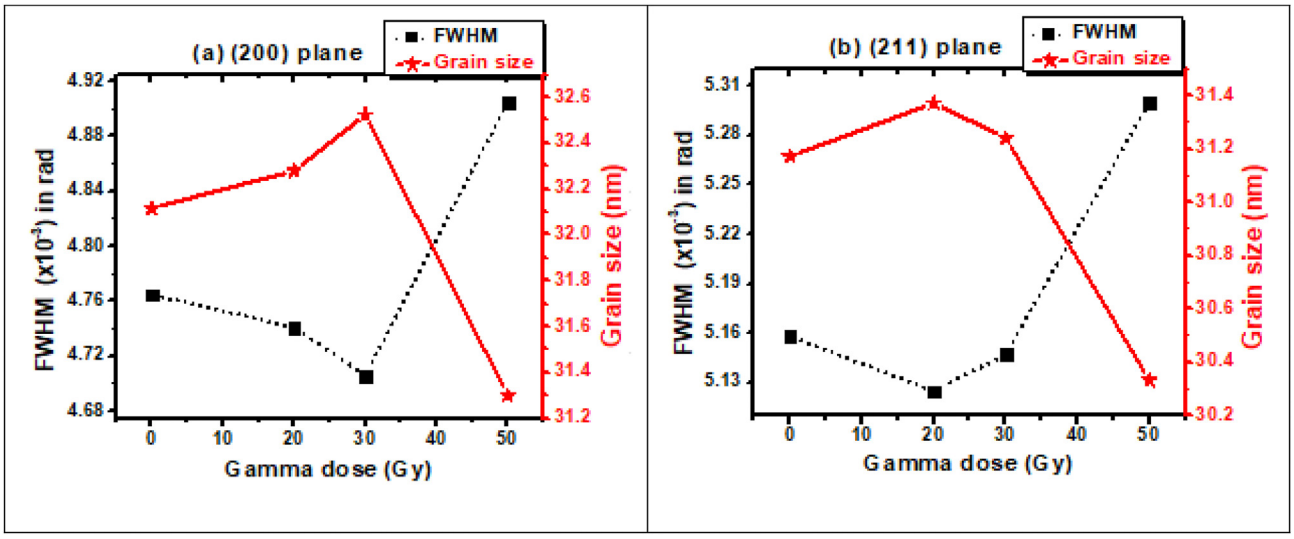

Fig. 5. Variations in grain size and FWHM of FTO films before irradiation (0 Gy) and after irradiation with 20, 30, and 50 Gy of γ-rays.

perfection of a crystal structure in terms of length of dislocation lines per unit volume of the crystal, and it represents the amount of defects in the sample (Bindu and Thomas, 2014; Kumar et al., 2016). The presence of dislocation defects in the structures of a crystalline material can strongly affect the properties of the material by interrupting the regular and periodic arrangement of atoms or molecules in the material (Sen et al., 2019b). The average dislocation density (δ) can be evaluated from the grain size (D) using the relation (Bindu and Thomas, 2014);

$$\delta = \frac{1}{D^2},$$

where D is the grain size.

It is noticed from Table 1 that both lattice strain and dislocation density exhibited similar behavior with increasing γ-ray dose. For the (200) plane, lattice strain and dislocation density decreased in samples irradiated with 20 Gy and 30 Gy before increasing when γ-dose was increased to 50 Gy. Whereas for the (211) plane, lattice strain and dislocation density decreased in the sample irradiated with 20 Gy and increased in samples exposed to 30 and 50 Gy. These observations imply reduction followed by increase in crystallographic defects in the films due to γ-irradiation. The observed decrease in lattice strain and dislocation density is attributed to γ-irradiation induced coalescence of small crystallites by grain boundary collapse which could have led to formation of large-sized crystallites that enhances the average grain size (Ahmed Ali et al., 2019; Choudhary and Chauhan, 2016; Sen et al., 2019b). This corresponds to the increase in spectral line intensity of the sample shown in Fig. 2. When the dose was further increased, the FTO crystallites seem to have broken down into comparatively smaller crystallites, and led to net decrease in the average grain size as observed in Fig. 5. This is responsible for the production and enhancement of crystal defects such as distortion and strain, and thus the low crystallinity enhancement rate at 50 Gy absorbed dose (Choudhary and Chauhan, 2016; Sudha et al., 2016). Thus, decreasing values of dislocation density and lattice strain ensure the improvement of crystallinity in the region of low γ-irradiation dose by decreasing the number of defects or imperfection in the crystal structures (Sen et al., 2019b). It is also clearly observed from Table 1 that dislocation density and strain are inversely proportional to grain size.

3.1.6. Lattice parameters

The variations in lattice constants "a" and "c" of the tetragonal FTO as a result of γ-irradiation were determined using the equation (Deyu et al., 2019);

$$\frac{1}{d_{hkl}^2} = \frac{h^2 + k^2}{a^2} + \frac{l^2}{c^2},$$

where d_{hkl} is the lattice spacing and h, k, and l are Miller indices.

The calculated results for lattice constants indicate that the lattice constants "a" and "c" exhibited opposite behaviors as seen in Table 1. For instance, the lattice constant "a" before irradiation was 4.7567 Å. But when the dose was increased to 20 Gy and 30 Gy, it decreased to 4.7544 Å and 4.7526 Å respectively. However, at 50 Gy, the lattice constant "a" increased to 4.7602 Å. For the case of lattice constant "c", it increased from 3.2075 before irradiation to 3.2108 Å and 3.2125 Å at 20 Gy and 30 Gy respectively, and later reduced to 3.2075 Å at 50 Gy dose. The obtained values of lattice constants are in same range with those obtained from the standard XRD card where a = 4.7382 Å and c = 3.1871 Å. The observed variations in lattice constants indicate that the material is experiencing stress and strain under irradiation (Mirzayev et al., 2019). Generally, these results reveal that the absorbed γ-ray doses used in this study remarkably modified the structural parameters of FTO without altering the basic crystal structure and that the 50 Gy γ-irradiation dose created point defects and active centres in the sample.

3.2. Morphological evolution of FTO under γ-irradiation

Atomic Force Microscope (AFM) was used to characterize the evolution in surface morphology of FTO film under γ-irradiation. Surface properties are important parameters to consider when choosing a material for a specialized application such as spacecraft thermal control coating. Fig. 6(a)-(d) shows the 2D micrographs and Fig. 7(a)-(d) shows the 3D micrographs of the original un-irradiated and γ-ray irradiated FTO films. Generally, notable changes in surface properties of the films in the form of overlapping hillocks are observed in samples exposed to 20 Gy and 30 Gy. Hillocks are formed when the incident γ-rays interact with target material and displace some of the sample's atoms, creating vacancies (Ahmed Ali et al., 2019). It's also clearly seen from Figs. 6 and 7(b)–(c) that there was reasonable increase in grain dimensions of films irradiated with 20 Gy and 30 Gy γ-ray doses. However, when the dose was further increased to 50 Gy, the film exhibited fine homogeneous grain structure with smooth and uniform surface structure evident from the observed decrease in porosity and disappearance of contrast peaks as seen in Fig. 6(d).

The morphological changes occurred when γ-rays bombarded FTO films and caused the well-shaped particles (grains) seen in the un-irradiated sample agglomerate into elongated type of structures with

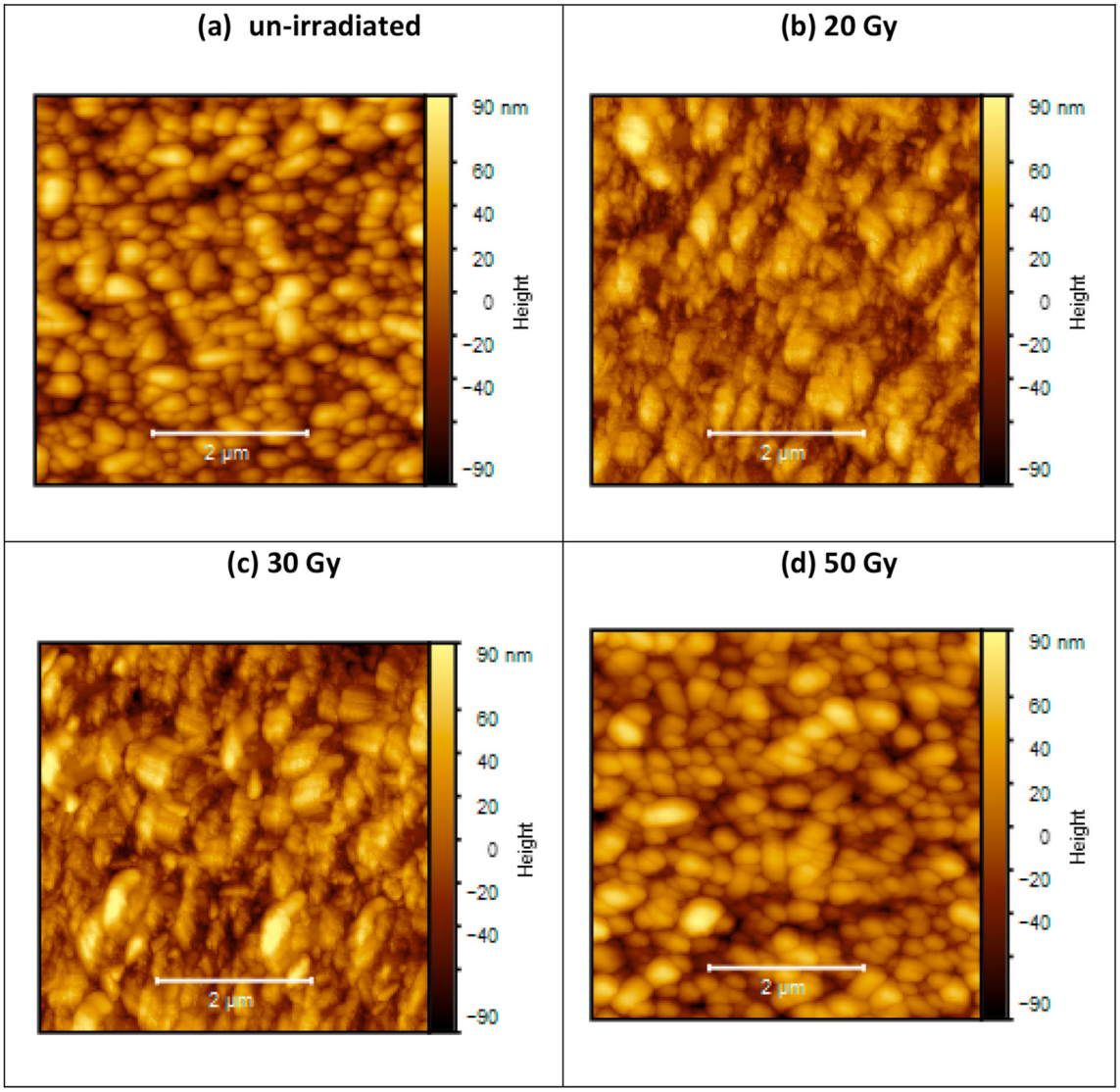

Fig. 6. 2D AFM images of un-irradiated and γ-irradiated FTO films at different doses.

bigger grain clusters and sizes as seen in Figs. 6 and 7(b)–(c). As already mentioned in the previous sub-section, interaction of γ-rays with matter results in irradiation induced lattice vibration, atomic displacement and local heating effects that can generate macro and micro repulsive or compressive stresses within the material (Kaya and Yilmaz, 2018). Presence of compressive stress causes swelling and reduction in grain boundary area (Adrovic, 2012; Kaya and Yilmaz, 2018). This could have resulted in the observed elongated grain structures of samples irradiated with 20 Gy and 30 Gy. Much as irradiation always lead to the creation of structural defects in materials, the healing effect of irradiation is also well known and reported (Arshak et al., 2004). In this study, irradiation healing effect was observed when γ-ray dose was increased to 50 Gy with a notable decrease in grain size and clear improvement in grain refinement of the FTO films as seen in Fig. 6(d). Such a material healing can be attributed to crumbling of particle structures as a result of irradiation induced repulsive stress which causes intrinsic defect recombination or reordering of initially disordered phase and aids the particles to regain their shapes (Adrovic, 2012; Arshak et al., 2004; Sen et al., 2019b). Healing effects normally occur at doses where the concentration of the induced defects do not exceed the concentration of intrinsic defects (Arshak et al., 2004). The observed refinement in grain sizes and shapes tend to suggest that for the current study maximum size is reached at 30 Gy. Further increase in dose beyond this resulted in the splitting of cluster due to energy transferred from the incoming radiation (Adrovic, 2012). Generally, the observed variations in grain properties suggest that grain sizes increased with dose up to 30 Gy and then decreased when dose was further increased to 50 Gy. This is in good agreement with the XRD results in Fig. 5.

Conversely, the average surface roughness (RMS) was found to decrease with increasing dose as shown in Fig. 7(a)–(d). The obtained results demonstrate that irradiation improved the surface roughness of the FTO thin films. The improvements in RMS values are attributed to the presence of irradiation induced repulsive stress in the films, which creates defects through atomic displacements and causes the surface atoms gain enough mobility to migrate towards the substrate, thereby decreasing the surface swelling (Adrovic, 2012; Ahmed Ali et al., 2019; Kaya and Yilmaz, 2018). Generally, it is worth concluding that the observed increase in grain size and decrease in surface roughness demonstrate that radiation exposure improves the film uniformity and density (Kaya and Yilmaz, 2018). It's on this basis that ionizing radiation is widely used for modifying the structure and properties of materials in order to enhance their performances either at bulk or surface levels (Lavanya et al., 2016).

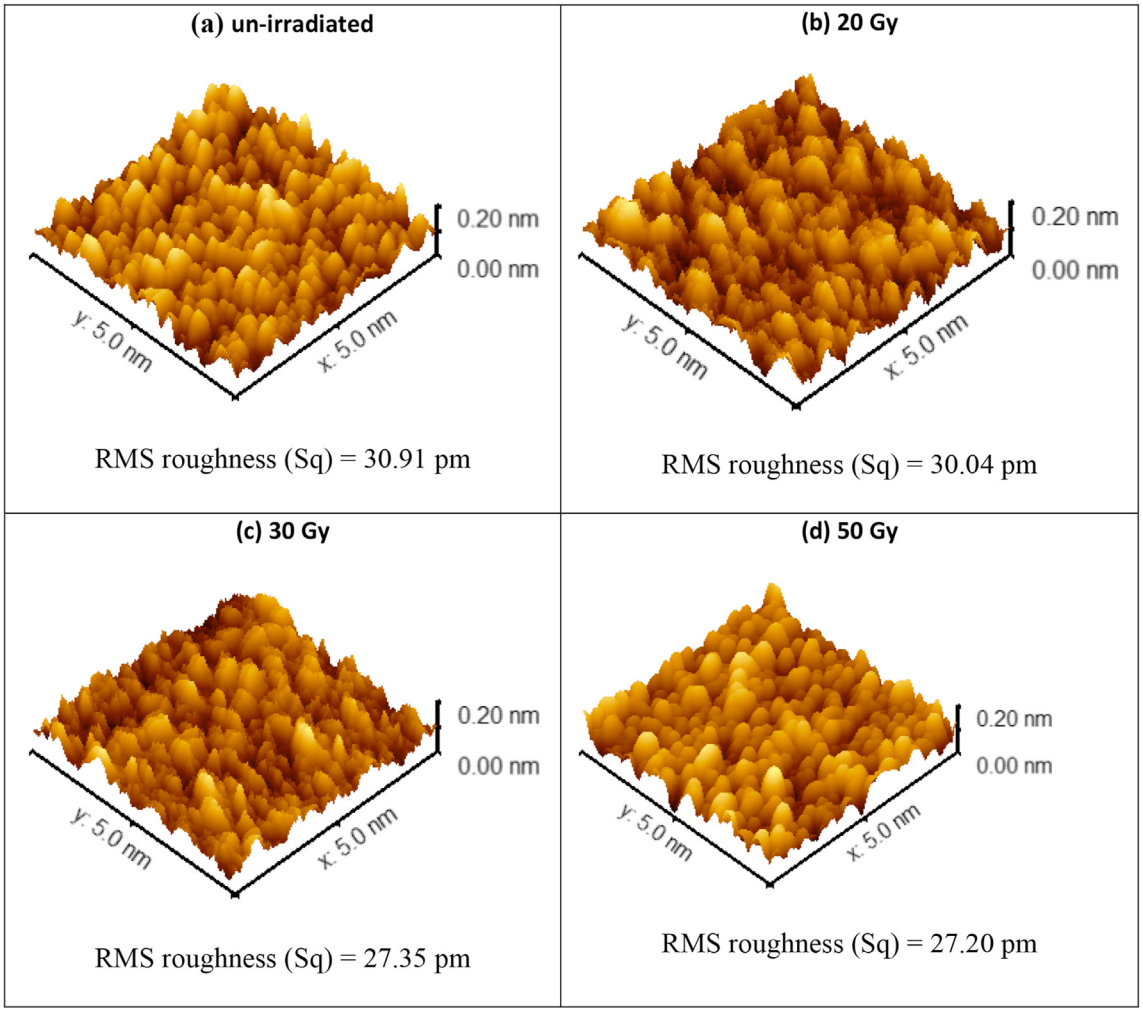

Fig. 7. 3D AFM images of un-irradiated and γ-irradiated FTO films at different doses.

3.3. Evolution in optical properties of FTO under γ-irradiation

Since the main goal of a spacecraft thermal control coating is either to confine heat within the spacecraft or reject heat back into space while keeping the temperatures of internal subsystems and components at optimal operation levels, it's imperative that evolutions in optical properties of FTO under irradiation be investigated in order to qualify it for such an application in future spacecraft. Ionizing radiations are known to degrade the optical properties of materials through formation and accumulation of irradiation induced color center defects (Abhirami et al., 2013). Formation of color centres is associated with an increase in electrical conductivity in which free electrons are produced as a result of band-to-band transitions and trapping of these electrons in oxygen ion vacancies (Duinong et al., 2019). The presence of color centres lead to increase in absorption or decrease in transmission of light through a matter. It's also associated with increase in carrier density in a material (Adrovic, 2012; Ahmed Ali et al., 2019). As seen in Fig. 8, the current study reports very slight distortion in optical transmittance of FTO thin films in the visible region (~400–1250 nm) and no variations in the infrared region (~1250–2500 nm) when exposed to low doses of γ-rays. Thus, the observed slight changes in transmittance in the visible region are due to irradiation induced formation and migration of color centres or vacancy defects within the FTO films. Generally, the result of this study indicate that the low γ-rays doses used did not cause reasonable damages to the optical properties of the FTO films.

4. Conclusion

The effects of low-dose gamma irradiation on crystalline structure, surface morphology, and optical transmittance properties of FTO have been studied. The investigation showed no amorphous phase transformations in the irradiated samples, and no new peaks of SnO_2 or diffraction patterns corresponding to fluoride phases such as SnF_2 were observed. Spectral line intensities of the irradiated films were significantly modified, with slight shifts in diffraction peak positons of the irradiated films. Also, there were clear variations in lattice parameters such as lattice spacing, grain size, lattice strain, and dislocation density of the irradiated films. The surface morphology of the samples were also modified as the surface roughness generally decreased with increasing dose and the grain structures of the samples varied significantly with dose. There were no significant impact on optical property, except that slight variations in transmittance were observed in the visible range of the spectrum. Generally, the above observations show that low-dose γ-irradiation caused significant changes in the structural and morphological properties, and insignificant changes in optical properties of FTO thin films.

CRediT authorship contribution statement

Bosco Oryema: Conceptualization, Methodology, Formal analysis, Investigation, Writing - original draft, Writing - review & editing, Visualization. **Edward Jurua:** Conceptualization, Validation, Writing - review & editing, Supervision, Project administration, Funding

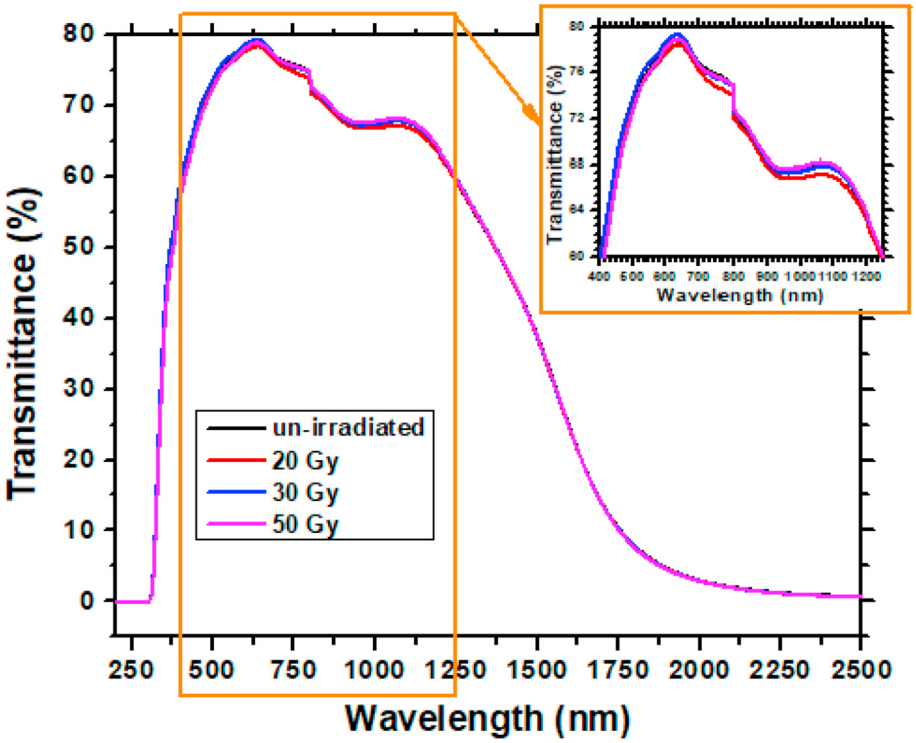

Fig. 8. Transmittance spectra of the un-irradiated and γ-irradiated FTO thin films.

acquisition. **Itani G. Madiba:** Conceptualization, Methodology, Validation, Resources, Writing - review & editing, Supervision. **Mlungisi Nkosi:** Conceptualization, Methodology, Formal analysis, Writing - review & editing. **Juliet Sackey:** Conceptualization, Methodology, Formal analysis, Writing - review & editing. **Malik Maaza:** Conceptualization, Methodology, Validation, Resources, Writing - review & editing, Supervision, Project administration, Funding acquisition.

Declaration of competing interest

The authors declare that they have no known competing financial interests or personal relationships that could have appeared to influence the work reported in this paper.

Acknowledgements

This work is supported by the International Science Program (ISP) through the Department of Physics, Mbarara University of Science and Technology, Uganda. We also acknowledge the Materials Research Department, National Research Foundation – iThemba LABS, South Africa for providing the necessary laboratory facilities for sample preparation, irradiation and characterization.

References

Abhirami, K.M., Sathyamoorthy, R., Asokan, K., 2013. Structural, optical and electrical properties of gamma irradiated SnO thin films. Radiat. Phys. Chem. 91, 35–39. https://doi.org/10.1016/j.radphyschem.2013.05.030.

Adjimi, A., Zeggar, M.L., Attaf, N., Aida, M.S., 2018. Fluorine-doped tin oxide thin films deposition by sol-gel technique. J. Cryst. Process Technol. 89–106. https://doi.org/10.4236/jcpt.2018.84006. 08.

Adrovic, F., 2012. Gamma radiation. Janeza Trdine 9, 51000 (Rijeka, Croatia).

Ahmed Ali, A.M., Ahmed, N.M., Mohammad, S.M., Sabah, F.A., Kabaa, E., Alsadig, A., Sulieman, A., 2019. Effect of gamma irradiation dose on the structure and pH sensitivity of ITO thin films in extended gate field effect transistor. Results Phys 12, 615–622. https://doi.org/10.1016/j.rinp.2018.10.066.

Alekperov, A.S., Jabarov, S.H., Mirzayev, M.N., Asgerov, E.B., Ismayilova, N.A., Aliyev, Y.I., Thabethe, T.T., Dang, N.T., 2019. Effect of gamma irradiation on microstructure of the layered Ge0.995Nd0.005S. Mod. Phys. Lett. B 33, 1–4. https://doi.org/10.1142/S0217984919501045.

Alyamani, A., Mustapha, N., 2016. Effects of high dose gamma irradiation on ITO thin film properties. Thin Solid Films 611, 27–32. https://doi.org/10.1016/j.tsf.2016.05.022.

Arshak, K., Korostynska, O., 2006. Response of metal oxide thin film structures to radiation. Mater. Sci. Eng. B 133, 1–7. https://doi.org/10.1016/j.mseb.2006.06.012.

Arshak, K., Korostynska, O., Clifford, S., 2004. Screen printed thick films of NiO and $LaFeO_3$ as gamma radiation sensors. Sensors Actuators, A Phys. 110, 354–360. https://doi.org/10.1016/j.sna.2003.08.011.

Baccini, D., 2019. Gamma irradiation response in photonic crystal and standard optical fiber Bragg grating sensors for radiation dosimetry. https://doi.org/10.1117/12.2539904.

Banyamin, Z.Y., Kelly, P.J., West, G., Boardman, J., 2014. Electrical and optical properties of fluorine doped tin oxide thin films prepared by magnetron sputtering. Coatings 4, 732–746. https://doi.org/10.3390/coatings4040732.

Batzill, M., Diebold, U., 2005. The surface and materials science of tin oxide. Prog. Surf. Sci. 79, 47–154. https://doi.org/10.1016/j.progsurf.2005.09.002.

Bindu, P., Thomas, S., 2014. Estimation of lattice strain in ZnO nanoparticles: X-ray peak profile analysis. J. Theor. Appl. Phys. 8, 123–134. https://doi.org/10.1007/s40094-014-0141-9.

Chancellor, J.C., Blue, R.S., Cengel, K.A., Auñón-Chancellor, S.M., Rubins, K.H., Katzgraber, H.G., Kennedy, A.R., 2018. Limitations in predicting the space radiation health risk for exploration astronauts. npj Microgravity 4, 1–11. https://doi.org/10.1038/s41526-018-0043-2.

Chancellor, J.C., Scott, G.B.I., Sutton, J.P., 2014. Space radiation: the number one risk to astronaut health beyond low earth orbit. Life 4, 491–510. https://doi.org/10.3390/life4030491.

Choudhary, R., Chauhan, R.P., 2016. Gamma irradiation induced modifications in spin coated CdSe thin films. J. Mater. Sci. Mater. Electron. 27, 674–681. https://doi.org/10.1007/s10854-016-5303-x.

Chowdhury, F.I., Blaine, T., Gougam, A.B., 2013. Optical transmission enhancement of fluorine doped tin oxide (FTO) on glass for thin film photovoltaic applications. Energy Procedia 42, 660–669. https://doi.org/10.1016/j.egypro.2013.11.068.

Deyu, G.K., Muñoz-Rojas, D., Rapenne, L., Deschanvres, J.L., Klein, A., Jiménez, C., Bellet, D., 2019. SnO_2 films deposited by ultrasonic spray pyrolysis: influence of Al incorporation on the properties. Molecules 24, 1–16. https://doi.org/10.3390/molecules24152797.

Duinong, M., Chee, F.P., Salleh, S., Alias, A., Mohd Salleh, K.A., Ibrahim, S., 2019. Structural and optical properties of gamma irradiated $CuGaO_2$ thin film deposited by radio frequency (RF) sputtering. J. Phys. Conf. Ser. 1358. https://doi.org/10.1088/1742-6596/1358/1/012047.

El-Nahass, M.M., Hassanien, A.M., Ashour, A., Alhuthali, A., Alomariy, S.E., Al-Baradi, A.M., Atta, A.A., 2018. Gamma irradiation effects on structural and optical properties of amorphous and crystalline Nb_2O_5 thin films. Opt. Quant. Electron. 50, 1–15. https://doi.org/10.1007/s11082-018-1580-3.

Gilmore, D.G., 2002. Spacecraft Thermal Control Handbook, second ed. .

Jiggens, P., Chavy-Macdonald, M.A., Santin, G., Menicucci, A., Evans, H., Hilgers, A., 2014. The magnitude and effects of extreme solar particle events. J. Sp. Weather Sp. Clim. 4. https://doi.org/10.1051/swsc/2014017.

Kadziołka-Gaweł, M., Dulski, M., Kalinowski, L., Wojtyniak, M., 2018. The effect of gamma irradiation on the structural properties of olivine. J. Radioanal. Nucl. Chem. 6, 261–268. https://doi.org/10.1007/s10967-018-5849-6.

Kaya, S., Abubakar, S., Yilmaz, E., 2019. Co-60 gamma irradiation influences on device characteristics of n-SnO_2/p-Si heterojunction diodes. Nucl. Instrum. Methods Phys. Res. B 445, 63–68. https://doi.org/10.1016/j.nimb.2019.03.013.

Kaya, S., Yilmaz, E., 2018. Modifications of structural, chemical, and electrical characteristics of Er_2O_3/Si interface under Co-60 gamma irradiation. Nucl. Instrum. Methods Phys. Res. Sect. B Beam Interact. Mater. Atoms 418, 74–79. https://doi.org/10.1016/j.nimb.2018.01.010.

Khamari, S.K., Dixit, V.K., Ganguli, T., Porwal, S., Singh, S.D., Kher, S., Sharma, R.K., Oak, S.M., 2011. Effect of ^{60}Co γ-ray irradiation on electrical properties of GaAs epilayer and GaAs p-i-n diode. Nucl. Instrum. Methods Phys. Res. Sect. B Beam Interact. Mater. Atoms 269, 272–276. https://doi.org/10.1016/j.nimb.2010.11.067.

Kondkar, V., Rukade, D., 2017. Au^{7+} ion irradiation induced phase transitions and morphological modifications in SnO_2 thin films. Int. J. Chem. Phys. Sci. 6, 9–17.

Kumar, N., Kumar, R., Kumar, S., Chakarvarti, S.K., 2016. Influence of ion beam irradiation induced defects on the structural, optical and electrical properties of tellurium nanowires. Mater. Chem. Phys. 183, 165–172. https://doi.org/10.1016/j.matchemphys.2016.08.015.

Kumari, M., Rana, P., Chauhan, R.P., 2014. Modifications in structural and electrical properties of gamma irradiated CdSe nanowires. Nucl. Instruments Methods Phys. Res. Sect. A Accel. Spectrometers, Detect. Assoc. Equip. 753, 116–120. https://doi.org/10.1016/j.nima.2014.03.062.

Langford, J., Wilson, A.J.C., 1978. Scherrer after sixty years: a survey and some new results in the determination of crystallite size. J. Appl. Crystallogr. 11, 102–113.

Lavanya, N., Sekar, C., Anithaa, A.C., Sudhan, N., Asokan, K., Bonavita, A., Leonardi, S.G., Neri, G., 2016. Investigations on the effect of gamma-ray irradiation on the gas sensing properties of SnO_2 nanoparticles. Nanotechnology 27, 1–9. https://doi.org/10.1088/0957-4484/27/38/385502.

Madiba, I.G., Émond, N., Chaker, M., Khanyile, B.S., Tadadjeu, S.I., Zolliker, P., Izerrouken, M., Matinise, N., Braun, A., Nkosi, M., Maaza, M., 2019. Effect of neutron irradiation on the structural, electrical and optical properties evolution of RPLD VO2 films. Nucl. Instrum. Methods Phys. Res. B 443, 25–30. https://doi.org/10.1016/j.nimb.2019.01.039.

Madiba, I.G., Émond, N., Chaker, M., Thema, F.T., Tadadjeu, S.I., Muller, U., 2017. Effects of gamma irradiations on reactive pulsed laser deposited vanadium dioxide thin films. Appl. Surf. Sci. 411, 271–278. https://doi.org/10.1016/j.apsusc.2017.03.131.

Maity, T.K., Sharma, S.L., 2011. Effects of gamma irradiation on electrical, optical and structural properties of tellurium dioxide thin films. Indian J. Pure Appl. Phys. 49, 606–612.

Meseguer, J., Pérez-Grande, I., Sanz-Andrés, A., 2012. Spacecraft Thermal Control. Woodhead Publishing Limited, Cambridge, UK.

Mirzayev, M.N., Jabarov, S.H., Asgerov, E.B., Mehdiyeva, R.N., Thabethe, T.T., Biira, S., Tiep, N.V., 2019. X-ray diffraction and thermodynamics kinetics of SiB_6 under gamma irradiation dose. Siliconindia 11, 2499–2504. https://doi.org/10.1007/s12633-018-0039-2.

Mirzayev, M.N., Jabarov, S.H., Asgerov, E.B., Mehdiyeva, R.N., Thabethe, T.T., Biira, S., Tiep, N.V., 2018. Crystal structure changes and weight kinetics of silicon-hexaboride under gamma irradiation dose. Results Phys 10, 541–545. https://doi.org/10.1016/j.rinp.2018.06.034.

Narula, C., Chauhan, R.P., 2018. High dose gamma ray exposure effect on the properties of CdSe nanowires. Radiat. Phys. Chem. 144, 405–412. https://doi.org/10.1016/j.radphyschem.2017.10.003.

Norberg, C., 2013. The space environment, human spaceflight and exploration. https://doi.org/10.1007/978-3-642-23725-6_3.

Pelton, J.N., Allahdadi, F., 2015. Handbook of cosmic hazards and planetary defense, handbook of cosmic hazards and planetary defense. https://doi.org/10.1007/978-3-319-03952-7.

Rani, S., Puri, N.K., Roy, S.C., Bhatnagar, M.C., Kanjilal, D., 2008. Effect of swift heavy ion irradiation on structure, optical, and gas sensing properties of SnO_2 thin films. Nucl. Instrum. Methods Phys. Res., Sect. B 266https://doi.org/10.1016/j.nimb.2008.02.062. 1987–1992.

Samad, W.Z., Salleh, M.M., Shafiee, A., Yarmo, M.A., 2011. Structural , optical and electrical properties of fluorine doped tin oxide thin films deposited using inkjet printing technique. Sains Malays. 40, 251–257.

Sen, S.K., Manir, M.S., Dutta, S., Ali, M.H., Khan, M.N.I., Matin, M.A., Hakim, M.A., 2019a. Influence of total absorbed dose of Co-60 γ-radiation on the properties of h-MoO_3 thin films. Thin Solid Films. https://doi.org/10.1016/j.tsf.2019.137700.

Sen, S.K., Noor, M., Al Mamun, M.A., Manir, M.S., Matin, M.A., Hakim, M.A., Nur, S., Dutta, S., 2019b. An investigation of ^{60}Co gamma radiation-induced effects on the properties of nanostructured α-MoO_3 for the application in optoelectronic and photonic devices. Opt. Quant. Electron. 51, 1–15. https://doi.org/10.1007/s11082-019-1797-9.

Sharma, A., Varshney, M., Verma, K.D., Kumar, Y., Kumar, R., 2013. Structural and surface microstructure evolutions in SnO thin films under ion irradiation. Nucl. Instrum. Methods Phys. Res. B 308, 15–20. https://doi.org/10.1016/j.nimb.2013.04.054.

Shi, X.H., Xu, K.J., 2017. Properties of fluorine-doped tin oxide films prepared by an improved sol-gel process. Mater. Sci. Semicond. Process. 58, 1–7. https://doi.org/10.1016/j.mssp.2016.09.038.

Singh, H.K., Avasthi, D.K., Aggarwal, S., 2015. Effect of swift heavy ion (SHI) irradiation on transparent conducting oxide electrodes for dye-sensitized solar cell applications. Nucl. Instrum. Methods Phys. Res. Sect. B Beam Interact. Mater. Atoms 353, 35–41. https://doi.org/10.1016/j.nimb.2015.04.031.

Souli, M., Bensalem, Y., Secu, M., Bartha, C., Enculescu, M., Mejri, A., Kamoun-Turki, N., Badica, P., 2019. Effect of high gamma radiations on physical properties of In_2S_3 thin films grown by chemical bath deposition for buffer layer applications. Results Phys 13. https://doi.org/10.1016/j.rinp.2019.02.051.

Sudha, A., Maity, T.K., Sharma, S.L., 2016. Effects of gamma irradiations on structural and electrical properties of indium oxide thin films prepared by thermal evaporation. Mater. Lett. 164, 372–375. https://doi.org/10.1016/j.matlet.2015.11.003.

Takahashi, A., Ikeda, H., Yoshida, Y., 2018. Role of high-linear energy transfer radiobiology in space radiation exposure risks. Int. J. Part. Ther. 151–159. https://doi.org/10.14338/IJPT-18-00013.1.

Tuğluoğlu, N., 2007. ^{60}Co γ-ray irradiation effects on the interface traps density of tin oxide films of different thicknesses on n-type Si (1 1 1) substrates. Nucl. Instrum. Methods Phys. Res. Sect. B Beam Interact. Mater. Atoms 254, 118–124. https://doi.org/10.1016/j.nimb.2006.10.082.

Tuyen, L.T.C., Jian, S.R., Tien, N.T., Le, P.H., 2019. Nanomechanical and material properties of fluorine-doped tin oxide thin films prepared by ultrasonic spray pyrolysis: effects of F-doping. Materials 12. https://doi.org/10.3390/ma12101665.

Wang, H., Sun, Y., Chu, J., Wang, X., Zhang, M., 2019. Intensive evaluation of radiation stability of phlogopite single crystals under high doses of γ-ray irradiation. RSC Adv. 9, 6199–6210. https://doi.org/10.1039/c8ra08565j.

Zeng, K., Zhu, F., Hu, J., Shen, L., Zhang, K., Gong, H., 2003. Investigation of mechanical properties of transparent conducting oxide thin films. Thin Solid Films 443, 60–65.